instruments

CITESCORE
2.6

Article

Mu2e Crystal Calorimeter Readout Electronics: Design and Characterisation

Nikolay Atanov, Vladimir Baranov, Leo Borrel, Caterina Bloise, Julian Budagov, Sergio Ceravolo, Franco Cervelli, Francesco Colao, Marco Cordelli, Giovanni Corradi et al.

Special Issue
Selected Papers from the 19th International Conference on Calorimetry in Particle Physics (CALOR 2022)

Edited by
Prof. Dr. Fabrizio Salvatore, Prof. Dr. Alessandro Cerri, Prof. Antonella De Santo and Prof. Iacopo Vivarelli

MDPI

https://doi.org/10.3390/instruments6040068

instruments

MDPI

Article

Mu2e Crystal Calorimeter Readout Electronics: Design and Characterisation

Nikolay Atanov [1], Vladimir Baranov [1], Leo Borrel [2], Caterina Bloise [3], Julian Budagov [1], Sergio Ceravolo [3], Franco Cervelli [4], Francesco Colao [3,5], Marco Cordelli [3], Giovanni Corradi [3], Yuri Davydov [1], Stefano Di Falco [4], Eleonora Diociaiuti [3], Simone Donati [4,6], Bertrand Echenard [2], Carlo Ferrari [4], Antonio Gioiosa [4], Simona Giovannella [3], Valerio Giusti [4,7], Vladimir Glagolev [1], Francesco Grancagnolo [8], Dariush Hampai [3], Fabio Happacher [3], David Hitlin [2], Matteo Martini [3,9], Sophie Middleton [2], Stefano Miscetti [3], Luca Morescalchi [4], Daniele Paesani [3,*], Daniele Pasciuto [4,6], Elena Pedreschi [4], Frank Porter [2], Fabrizio Raffaelli [4], Alessandro Saputi [10], Ivano Sarra [3], Franco Spinella [4], Alessandra Taffara [4], Anna Maria Zanetti [11] and Ren-Yuan Zhu [2]

1 Joint Institute for Nuclear Research, 141980 Dubna, Russia
2 California Institute of Technology, Pasadena, CA 91125, USA
3 Laboratori Nazionali di Frascati dell'INFN, 56100 Pisa, Italy
4 INFN—Sezione di Pisa, 56100 Pisa, Italy
5 ENEA—Frascati, 00044 Frascati, Italy
6 Department of Physics, University of Pisa, 56100 Pisa, Italy
7 Department of Civil and Industrial Engineering, University of Pisa, 56100 Pisa, Italy
8 INFN—Sezione di Lecce, 73100 Lecce, Italy
9 Department of Engineering Sciences, Guglielmo Marconi University, 00193 Roma, Italy
10 INFN—Sezione di Ferrara, 44100 Ferrara, Italy
11 INFN—Sezione di Trieste, 34149 Trieste, Italy
* Correspondence: daniele.paesani@lnf.infn.it

Abstract: The Mu2e experiment at Fermi National Accelerator Laboratory will search for the charged-lepton flavour-violating neutrinoless conversion of negative muons into electrons in the Coulomb field of an Al nucleus. The conversion electron with a monoenergetic 104.967 MeV signature will be identified by a complementary measurement carried out by a high-resolution tracker and an electromagnetic calorimeter, improving by four orders of magnitude the current single-event sensitivity. The calorimeter—composed of 1348 pure CsI crystals arranged in two annular disks—has a high granularity, 10% energy resolution and 500 ps timing resolution for 100 MeV electrons. The readout, based on large-area UV-extended SiPMs, features a fully custom readout chain, from the analogue front-end electronics to the digitisation boards. The readout electronics design was validated for operation in vacuum and under magnetic fields. An extensive radiation hardness certification campaign certified the FEE design for doses up to 100 krad and 10^{12} n_{1MeVeq}/cm^2 and for single-event effects. A final vertical slice test on the final readout chain was carried out with cosmic rays on a large-scale calorimeter prototype.

Keywords: calorimeter; front-end; electronics; crystals; SiPM; MPPC; flavour violation

check for updates

Citation: Atanov, N.; Baranov, V.; Borrel, L.; Bloise, C.; Budagov, J.; Ceravolo, S.; Cervelli, F.; Colao, F.; Cordelli, M.; Corradi, G.; et al. Mu2e Crystal Calorimeter Readout Electronics: Design and Characterisation. *Instruments* **2022**, *6*, 68. https://doi.org/10.3390/instruments6040068

Academic Editors: Fabrizio Salvatore, Alessandro Cerri, Antonella De Santo and Iacopo Vivarelli

Received: 6 September 2022
Accepted: 9 October 2022
Published: 20 October 2022

Publisher's Note: MDPI stays neutral with regard to jurisdictional claims in published maps and institutional affiliations.

1. Introduction

The Mu2e experiment [1] at Fermilab will search for the charged-lepton flavour-violating (CLFV) process of the muon to electron conversion in the Coulomb field of aluminium nuclei, aiming to improve by four orders of magnitude the current single-event sensitivity, by means of a high-intensity pulsed muon beam and high-performance detectors—a high-resolution (<200 keV/c) straw-tube tracker in conjunction with an electromagnetic calorimeter (EMC)—to identify the distinctive signal signature, represented by a monoenergetic conversion electron of 104.96 MeV, slightly below the muon mass. The EMC complements the tracker providing high rejection power in μ/e separation, cluster-seeding

for tracking algorithms, while also providing stand-alone online trigger capabilities. The calorimeter needs to maintain high levels of performance and stability while operating in a high vacuum, in the presence of a 1 T magnetic field and in a harsh radiation environment. The EMC has high granularity, good energy (<10%) and timing (<500 ps) resolution for 100 MeV electrons [2]. It is composed of two disks, each housing a matrix of 674 parallelepipedonal ($34 \times 34 \times 200$ mm^3) undoped CsI crystals. Each is read out by two large-area arrays of UV-extended silicon photomultipliers (SiPMs) and a fully custom signal chain. The design, validation and qualification steps relative to the calorimeter front-end electronics are reported in the following sections, while a detailed description of the Mu2e experiment, its calorimeter and the associated construction status can be found elsewhere in the current issue [3]. The Mu2e experiment is currently under construction at Fermilab. Detector commissioning and installation in the experimental hall will begin in late 2023.

2. Readout and Signal Chain Architecture

The Mu2e calorimeter employs a fully custom readout chain for 2716 channels. Behind the crystal matrices, 1348 readout units (ROU) are installed. A total of 136 mezzanine boards (MB) and 136 digitiser readout controllers (DiRAC) are installed in 20 crates embedded in the calorimeter's mechanical structure (Figure 1).

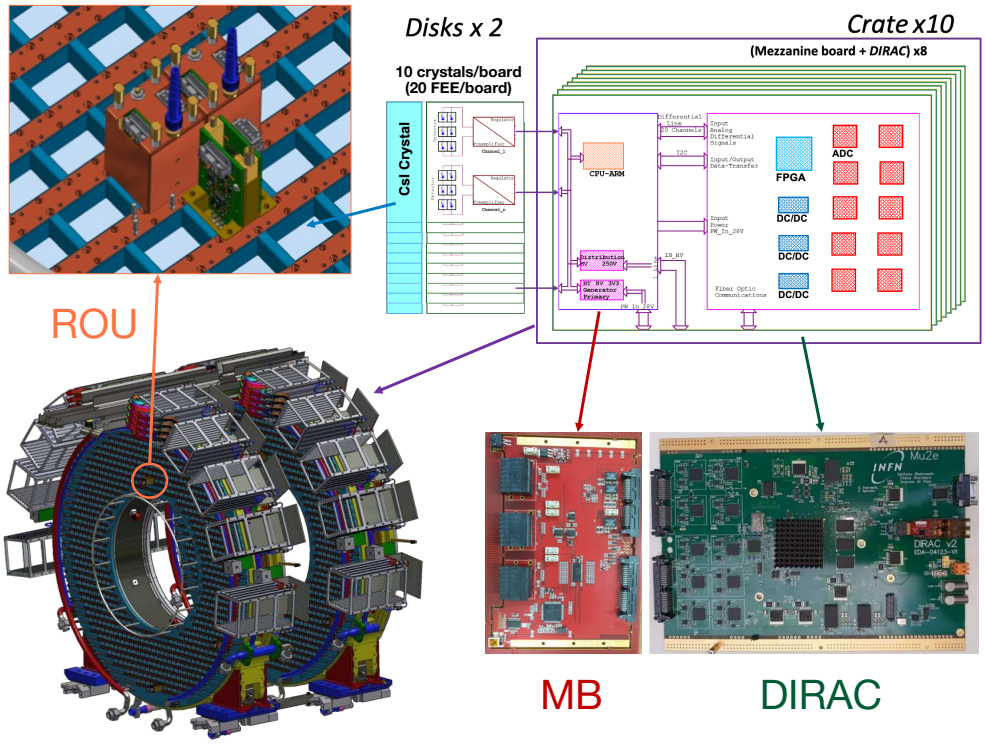

Figure 1. Overview of the Mu2e calorimeter readout system. Top-left: detail of the readout units (ROU) assembly in the calorimeter disk (heat exchangers are also visible). The electronics crates' architecture, including mezzanine (MB) and DiRAC boards, is also shown on the right.

2.1. Readout Units

Each ROU houses two fully independent readout channels per crystal, each comprising two custom large-area UV-extended SiPMs and the relative front-end electronics (FEE) boards. The SiPMs are glued on copper holders (Figure 2, left) which are thermally coupled to the cooling system (Figure 1, top-left) for their thermalisation down to −10 °C, to cope with the nonionising-dose-induced dark current increase.

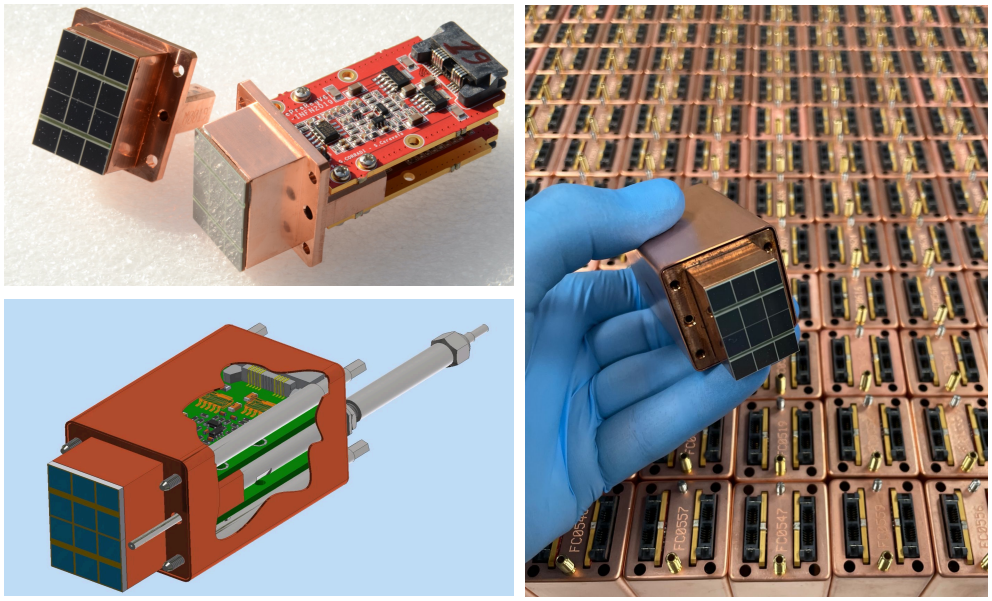

Figure 2. Bottom-left: rendering of an ROU, fibre-optic needle holder and Faraday cage are shown. **Top-left**: SiPM holder and FEE assembly. **Right**: ROUs from production lots.

A 2 mm gap is present between crystals and SiPMs to reduce their thermal coupling, preventing gradients along the crystal axis which could worsen their longitudinal response uniformity. A fibre-optic holder (Figure 2, bottom-left) allows for the distribution of 520 nm picosecond laser pulses for photosensor gain monitoring and timing alignment. A copper Faraday cage completes the assembly.

2.2. SiPMs

Two adjacent custom SiPMs by Hamamatsu [4] are used for each crystal. Each photodetector (Figure 2) consists of a 2×3 array of 6×6 mm^2 SiPMs with 50 µm pixels. The photodetectors are UV-extended to better match the 315 nm spectral peak of pure CsI.

2.3. FEE Boards

FEE boards installed directly behind each photosensor (Figure 2, top-left) perform signal amplification and shaping, while also managing all slow control functions. The six cells of each photosensor are connected in two series of three elements, to decrease their equivalent capacitance, and two grounded-base BJT stages form a fast current adder with $\sim$30 Ω input impedance for each series (Figure 3). A second amplification stage drives a pole-zero cancellation network followed by a shaping section consisting in a 3-pole pulse stretcher based on a Bessel filter. Pulse stretching allows one to shape the pulse rising edge to approximately 25 ns to allow an optimal signal reconstruction. A balanced line driver transmits SiPM pulses to the DiRAC digitiser with a 2 V dynamic range. The overall system gain (1 or 2) can be set via a dedicated jumper.

The nominal 1 MHz rate capability of the analogue section allows one to cope with the high experimental hit rate.

A custom high-stability, low-ripple high-voltage linear regulator provides individual bias voltages up to 200 V—programmable in 50 mV increments via the on-board SPI DAC—with a nominal current capability of 2 mA per SiPM. Integrated bias, current and temperature monitors are also present, with dedicated 12-bit SPI ADC channels.

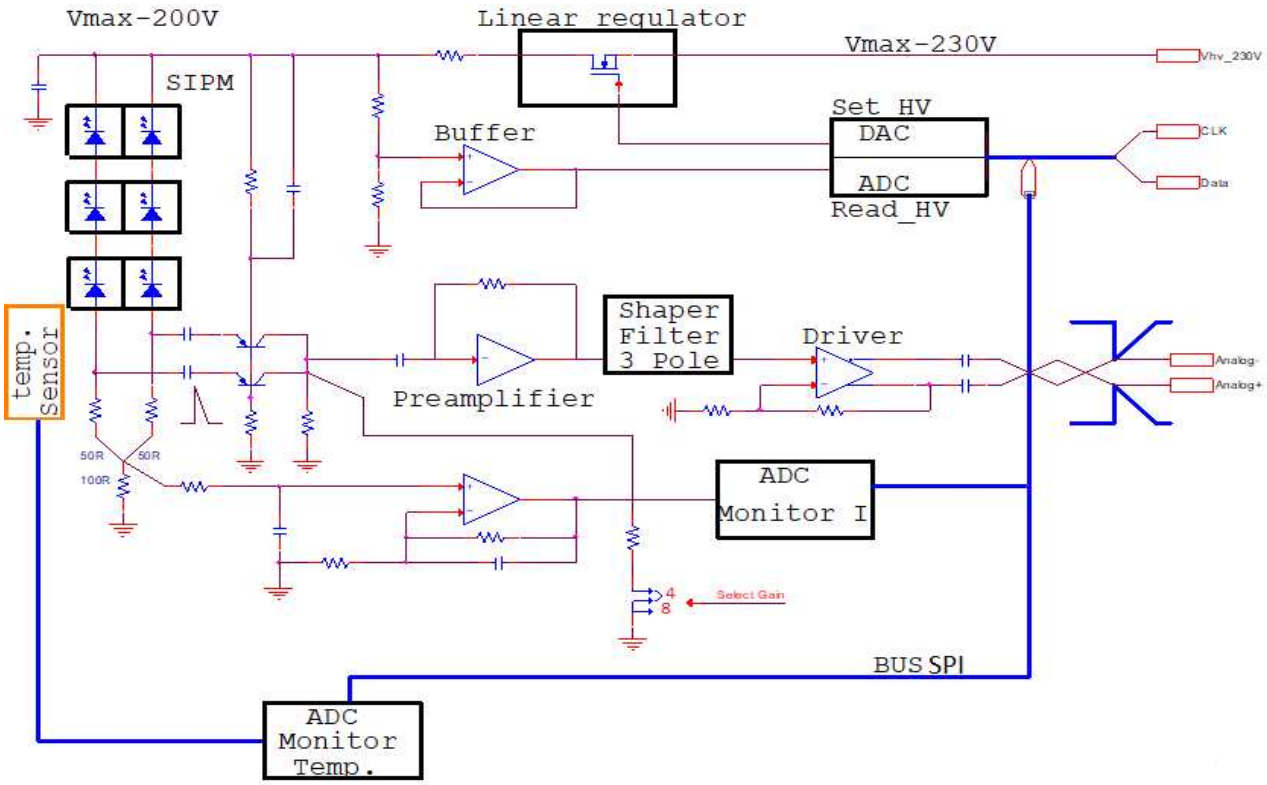

Figure 3. Block schematic of the FEE board architecture. The signal amplification and shaping, along with the integrated slow control functions, are shown.

2.4. Mezzanine Boards

Mezzanine boards employing ARM microprocessors perform the power distribution (low- and high-voltage) to all ROUs and manage all slow control functions to the FEE via the dedicated SPI bus and multiplexer.

2.5. DiRAC

Each DiRAC board employs a PolarFire rad-hard FPGA and allows one to digitise 20 calorimeter channels at 200 Msps via 12-bit Flash ADCs. A VTRX-based 10 Gsps optical link allows a data stream and slow control management with the Mu2e trigger and data acquisition system (TDAQ) [5]. Full signal digitisation allows one to better cope with the high expected pile-up rates. More on the design and construction status of the DiRAC boards can be found elsewhere [6,7].

2.6. Signal Reconstruction

Timing and charge reconstruction, along with pile-up disentangling, are carried out on sampled pulses by means of a template fit algorithm, using a 3-parameter optimisation. To compensate any channel-to-channel signal variation, individual waveform templates—sets of interpolated nodes with fixed proportion—are generated for each channel by aligning and averaging a large dataset of sampled hits (Figure 4). Templates can then be fitted using a three-parameter optimisation (wave baseline, wave timing offset and scale). The timing fit parameter is used as a timing reference for the characterisation studies hereby reported.

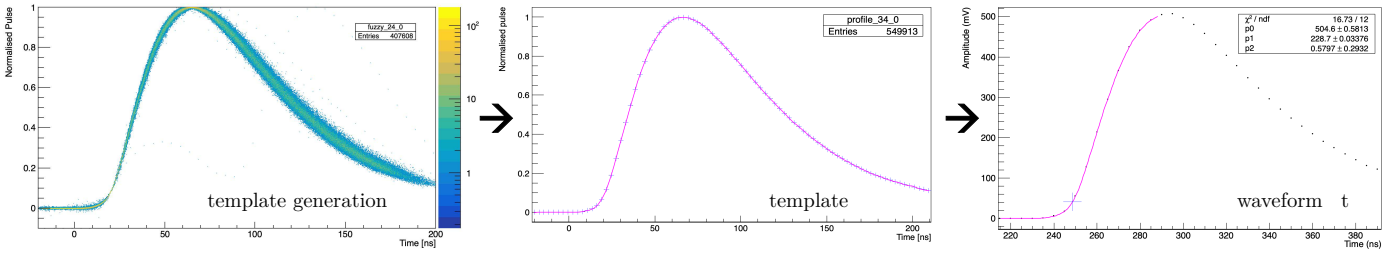

Figure 4. Example of template generation and waveform fitting for a calorimeter channel.

3. Qualification and QC

3.1. SiPM

An intense QC campaign was carried out on production SiPMs, including measurements of V_{br}, I_{dark} and PDE, and their relative spread over the six cells of the photosensor. It was verified that the SiPM's gain and pulse shape remained unaltered after exposure to 100 krad and 10^{12} n_{1MeVeq}/cm^2. The maximum allowed 2.5 mA dark current following irradiation and a mean time to failure MTTF > 10^7 h at 20 °C were verified on all production batches. The quality control on production SiPMs ended in late 2019 with less than 2% out-of-spec components. The main results are summarised in Figure 5. Further details can be found elsewhere [8].

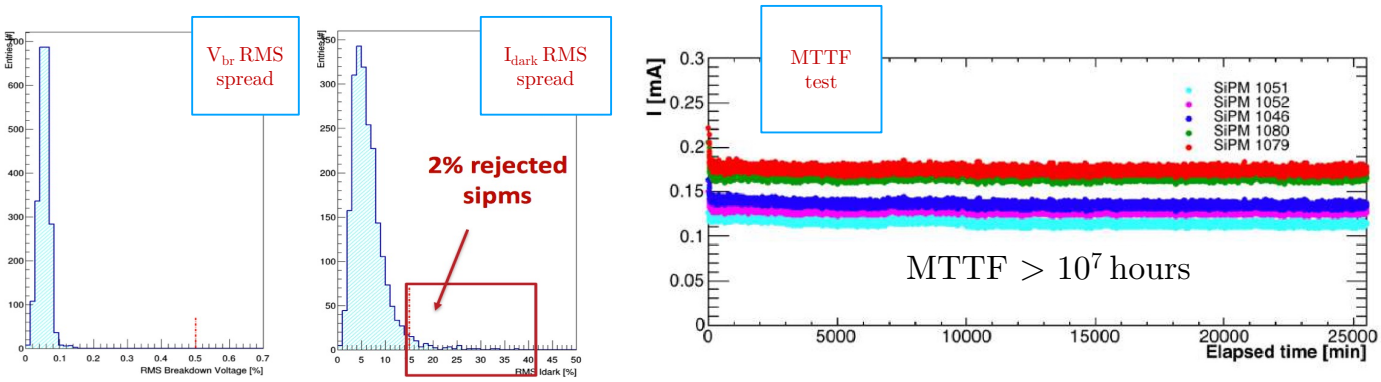

Figure 5. Summary of breakdown voltage (**left**) and dark current (**centre**) RMS spread in production lots. Summary of MTTF tests on production SiPMs (**right**): dark current as a function of elapsed operating time.

3.2. Electronics Qualification Steps

General qualification steps for the FEE, MB and DiRAC comprised tests carried out to validate performance with respect to the harsh Mu2e operating environment, with a particular attention to radiation hardness performance, as discussed later. Tests with B-fields were carried out at the Argonne National Laboratory [9] on the FEE, MB and DiRAC (Figure 6, top-right), with a focus on the buck converter operation and efficiency. Tests in vacuum were carried out on the MB, FEE and DiRAC. Quality control tests on production FEEs and MBs included burn-in tests at 65 °C, along with calibration of the HV regulator and temperature/current sensing circuitry (Figure 6). Signal shape and gain linearity were also assured by pulsing the analogue section with a dedicated signal injection setup.

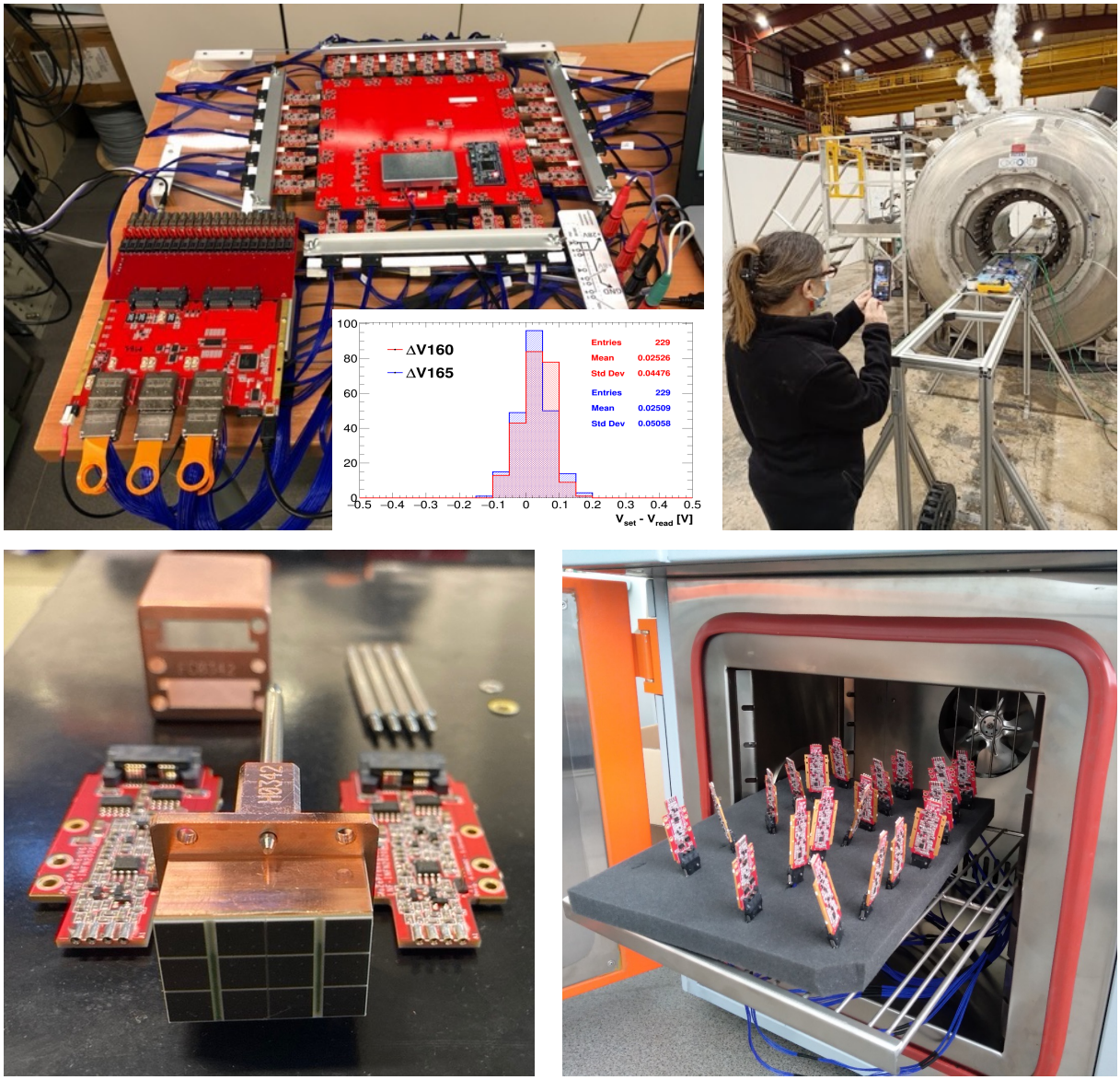

Figure 6. FEE QA bench (**top-left**), calibration results for HV regulator output are also shown. Test in magnetic fields at Argonne National Laboratory (**top-right**). ROU before assembly with the FEE boards (**bottom-left**). FEE burn-in test (**bottom-right**).

3.3. Readout Units QC

An automated testing station was developed at LNF-INFN to perform QC steps on production ROUs [10]. As shown in Figure 7, a 420 nm nanosecond UV LED source was pulsed at kHz repetition rate over two assembled ROUs at a time. A motorised neutral density filter selector was used to vary the source intensity.

The SiPM gain was evaluated as $G = \sqrt{p_0}/(q_e[pC])$ from the fit $\frac{\sigma_Q}{Q} = \frac{p_0}{\sqrt{Q}} \oplus \frac{p_1}{Q} \oplus p_2$, also shown in Figure 7. The SiPM response was calibrated—and stored in a dedicated ROU database—for different overvoltages and operating temperatures. An overall gain spread <3% RMS was observed in production. A reproducibility better than 1.5% was observed during the station operation.

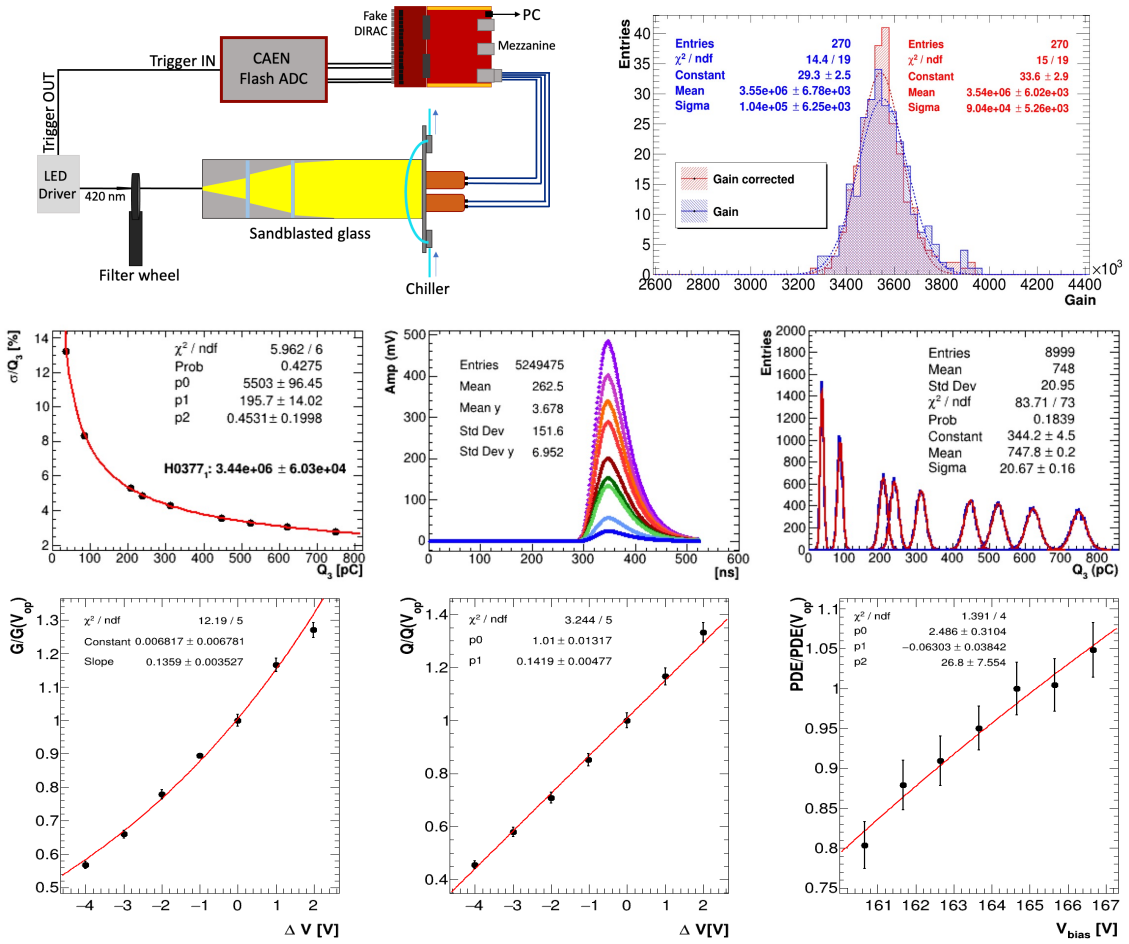

Figure 7. Top-left: test station architecture, including light pulse generator and attenuator. **Top-right**: distribution of ROU gains for a production batch. **Centre**: example of SiPM waveforms (**middle**) and charges (**right**) for various LED source amplitudes. **Centre-left**: σ_Q/Q fit. **Bottom**: gain, charge and PDE scans at various overvoltages.

4. Irradiation Tests of the Readout Electronics

4.1. Radiation Environment and Requirements

A full simulation of the Mu2e radiation environment was carried out via MARS15 and FLUKA. The electronic boards were mocked by equivalent boxes containing a compound of Si, Au, Al, Cu and polyethylene. Worst-case requirements for the EMC electronics (upstream disk, inner region) were set to 100 krad (inclusive of a safety factor of 12) and 3×10^{12} n_{1MeVeq}/cm^2 for (inclusive of a safety factor of 6) for 5 years of operation. The reference high-energy (>20 MeV) hadron flux for single-event effects (SEE) validation was set to 1×10^{10} p/cm^2.

4.2. Ionising Dose Campaign

All total ionising dose (TID) qualification steps for the FEE and MB were carried out at ENEA-Calliope, a pool-type, high-intensity ^{60}Co source. After a 2-year-long campaign, the final choice of FEE rad-hard SPI ADCs and DACs (ADC1280S022CIMT and 121S101CIMKX, both from Texas Instruments) was confirmed with a final test in 2020, in which a total of six FEE boards from controlled production lots were irradiated up to 105 krad (0.85 krad/h dose-rate) in different operating configurations (Figure 8). All slow control monitoring channels exhibited excellent stability throughout the test with a maximum absolute drift of 2 LSB, comparable with the case of nonirradiated boards. The stability of the regulated high voltage was better than 0.1 % at a nominal 160 V. Similar tests with ionising dose on

the MB were also performed to validate the hardness of the microprocessor and the SPI communication, along with the stability and efficiency of the onboard buck converters. No detrimental effects were observed for the 25 krad TID MB requirement.

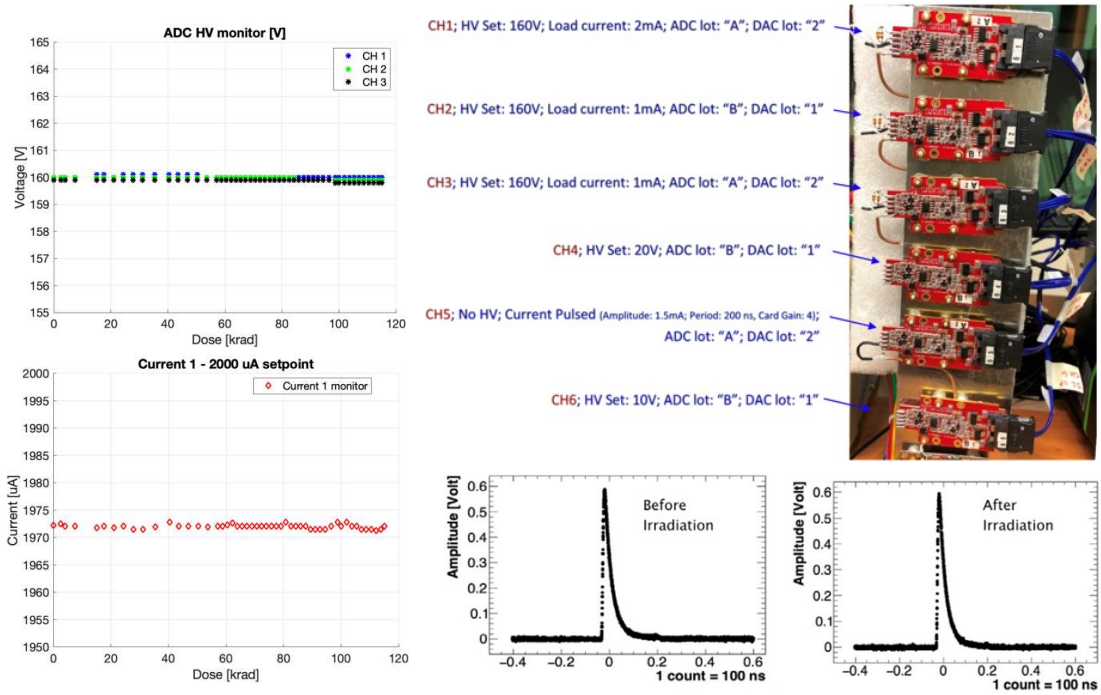

Figure 8. Top-right: configuration for the final FEE TID test. **Left**: example of stability plots for regulator voltage and current during irradiation. **Bottom-right**: waveforms comparison before and after TID irradiation.

4.3. Nonionising Dose Campaign

Tests were carried out at ENEA-FNG [11], utilising a 14 MeV neutron gun based on T(d,n)α fusion. Separate runs were carried out on the FEE and MB boards. No failure or performance degradation was observed in both cases due to cumulative nonionising dose damage after the delivery of an equivalent 3×10^{12} n_{1MeVeq}/cm^2 fluence over the course of 5 h.

4.4. Single-Event Effects

Dedicated studies for SEE have been carried out and are in progress on the MB processor and the DiRAC FPGA, to study firmware functionality, memory and communication corruption in the DiRAC–MB–FEE chain. The measurement of single-event upset (SEU) and latch-up (SEL) cross sections is crucial for the estimation of the expected functional interrupt rate under the high-energy hadrons exposures during experimental runs, and to optimise the implementation of hardware (power supply latch-up protection, watchdogs and dedicated reset lines) and firmware (scrubbing, memory and data integrity checks) countermeasures.

With respect to the MB processor, a preliminary simulation was carried out on-bench by fault-injection, accessing the processor memory via JTAG and performing random single or multiple bit flips while running the usual slow control functions, while first SEE data were taken during the aforementioned runs at ENEA-FNG (Figure 9, left) to validate the mitigation techniques effectiveness: the occurrence of approximately one SEU-related functional interrupt every 2×10^{10} n_{1MeVeq}/cm^2 delivered on the MB processor was observed, and it was verified that the board could correctly detect and recover operations via reset or power cycling. Similar tests were carried out for the FEE and DiRAC boards. The final validation tests for SEE on the FEE–MB–DiRAC chain are being carried out, at the moment

of writing, using a 200 MeV proton beam at the Northwestern Medicine Warrenville Proton Center, US (Figure 9, right). These data will provide the correct estimation of the expected mean time between functional interrupts for each board, along with the validation of the SEL protection and other countermeasures.

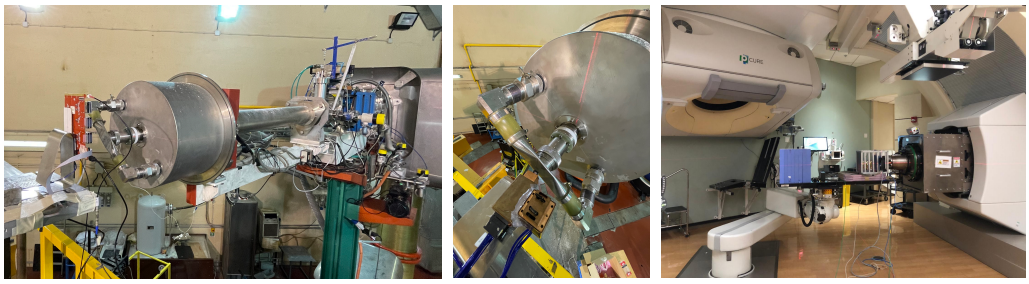

Figure 9. ENEA-FNG facility during MB irradiation (**left**) and ROU irradiation (**centre**). Northwestern Medicine Warrenville Proton Center (**right**).

5. Readout Chain Vertical Slice Test

In late 2021 a vertical slice test (VST) of the full calorimeter read out chain was performed with cosmic muons at LNF-INFN on the calorimeter Module-0 [3] (Figure 10, right), a large-scale prototype counting 51 crystals and designed with the final configuration of all detector services and subsystems (mechanics, cooling system, laser calibration system and vessel for vacuum operation).

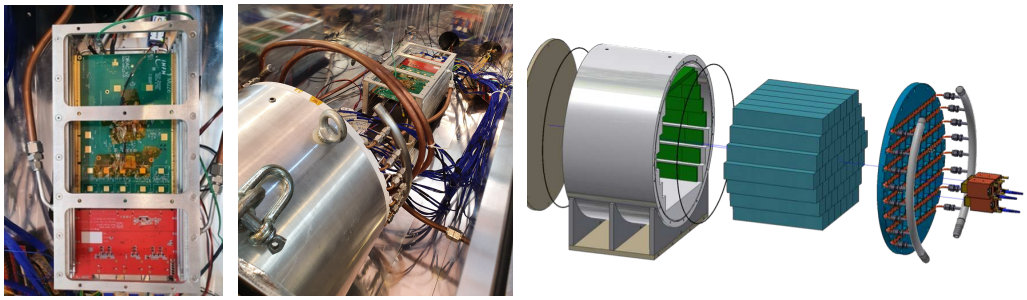

Figure 10. Centre: VST setup with Module-0 and electronics crate. **Left**: detail of MB and DiRAC installed in the electronics crate. **Right**: Module-0 architecture.

For the VST, an electronics crate with a DiRAC and an MB board—and the respective cooling systems—were installed inside the Module-0 vacuum vessel to read out a total of 20 FEE channels (Figure 10, left). The 17 innermost crystals were instrumented with production ROUs, and a dual readout was used for the central and the central uppermost/lowermost crystals.

Triggering was performed either via the coincidence of two scintillator plates placed above and below the Module-0, or via the DiRAC onboard autotrigger, for which a minimum hit number of three crystals was set. The energy response was equalised online acting on SiPM biases to a level <5% and further offline equalisation was performed on the minimum ionizing particles (MIP) most probable 21 MeV deposit (Figure 11, left). The pedestals were characterised for all channels (Figure 12, right), yielding a $\sim$200 keV worst-case equivalent noise. The SiPM gain stability was checked against the MIP peak, and its fluctuations were compatible with the ± 1 °C stability of the temperature regulation system (Figure 12, left).

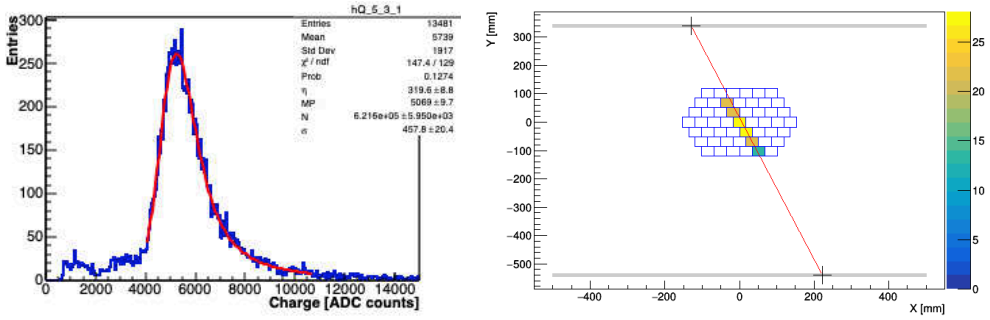

Figure 11. Example of MIP deposits in a crystal during VST with superimposed Landau–Gauss convolution fit (**left**). Example of MIP track reconstructed in the crystal matrix plane (**right**); colour scale represents energy deposit in MeV.

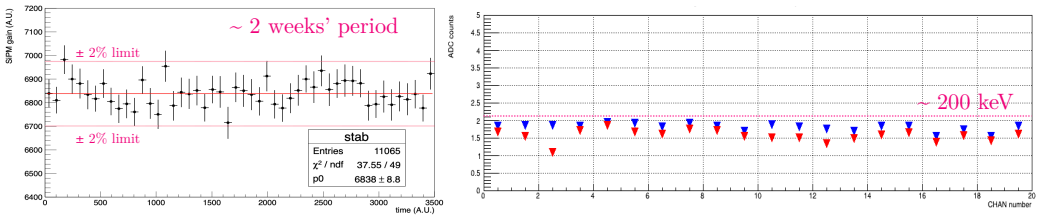

Figure 12. Relative SiPM gain stability over 2 weeks against MIP peak for the central channel (**left**). Charge pedestals expressed in ADC counts RMS for all Module-0 channels for two subsequent runs (blue and red colours).

The MIP tracks inside the calorimeter were reconstructed with a 2D fit in the plane orthogonal to the crystal axes (Figure 11, right) and an iterative algorithm was used to calculate an energy-weighted time centroid for each event and adjust the relative timing offset between channels, accounting for the relative 2D time-of-flight (ToF) corrections, resulting in a relative alignment better than 5 ps RMS after five iterations (Figure 13, left). A mean time resolution of order 210 ps was evaluated with MIPs for individual crystals, from the time difference between the left and right channels of the corresponding ROU, as shown for the central crystal in Figure 13, top-left.

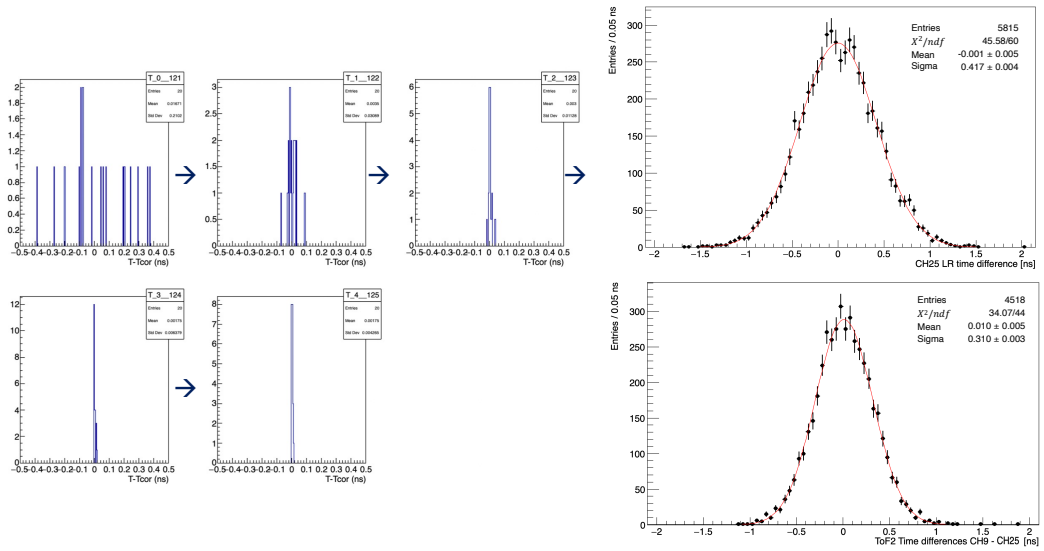

Figure 13. Overview of the timing alignment procedure (**left**): histogram of offset residuals after 5 iterations of the alignment algorithm. **Top-right**: example distribution of MIP timing differences between the left and right channels of the dual readout for the central crystal. **Bottom-right**: example of timing differences between two channels after 2D ToF correction and timing alignment.

The timing difference distributions between channels, after ToF correction, were well centred around zero (Figure 13, bottom-left), and their sigma scales well within the quadrature sum of the individual timing resolution terms previously obtained, apart from a minor spread, associated to the ToF contribution due the unknown track slope along the calorimeter axis. An algorithm to reconstruct this slope from the optical transport timing differences on the crystal matrix is currently being developed for increased performance. The timing results were similar for the other instrumented channels. Finally, the mean timing resolution dependence on energy over the MIP energy range is shown in Figure 14 for the central channel.

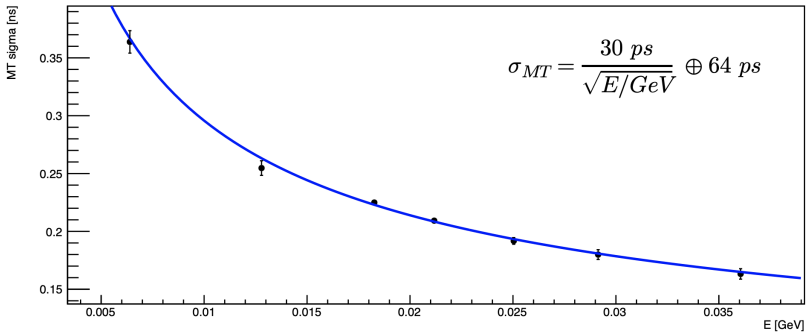

Figure 14. Central crystal mean time resolution for different energy slices (central channel).

6. Summary

The Mu2e calorimeter has fully custom readout electronics, from SiPM to digitiser. The design of the FEE, mezzanine boards, and DiRAC digitiser boards were validated after an intense and prolonged qualification campaign, to assess their performance and compliance to the requirements under the Mu2e operating conditions, featuring a high vacuum, 1 T B-Field and a harsh radiation environment. The production of all FEE was completed in 2021, and the ROU assembly and QC are in progress. The final SEE tests are in progress for the MB and DiRAC boards, prior to their production launch.

Author Contributions: All the work was carried out by the Mu2e Calorimeter group. All authors have read and agreed to the published version of the manuscript.

Funding: The present research was funded and supported by all institutions listed in the Acknowledgments section below.

Data Availability Statement: Not applicable.

Acknowledgments: We are grateful for the vital contributions of the Fermilab staff and the technical staff of the participating institutions. This work was supported by the US Department of Energy; the Istituto Nazionale di Fisica Nucleare, Italy; the Science and Technology Facilities Council, UK; the Ministry of Education and Science, Russian Federation; the National Science Foundation, USA; the Thousand Talents Plan, China; the Helmholtz Association, Germany; and the EU Horizon 2020 Research and Innovation Program under the Marie Sklodowska-Curie grant agreement nos. 101003460, 101006726, 734303, 822185 and 858199. This document was prepared by members of the Mu2e Collaboration using the resources of the Fermi National Accelerator Laboratory (Fermilab), a U.S. Department of Energy, Office of Science, HEP User Facility. Fermilab is managed by the Fermi Research Alliance, LLC (FRA), acting under contract no. DE-AC02-07CH11359.

Conflicts of Interest: The authors declare no conflict of interest.

References

1. Bartoszek, L.; Barnes, E.; Miller, J.P.; Mott, J.; Palladino, A.; Quirk, J.; Roberts, B.L.; Crnkovic, J.; Polychronakos, V.; Tishchenko, V.; et al. The Mu2e Collaboration, Mu2e technical design report. *arXiv* **2015**, arXiv:1501.05241.
2. Atanov, N.; Baranov, V.; Budagov, J.; Caiulo, D.; Cervelli, F.; Colao, F.; Zhu, R.Y. Design and test of the Mu2e un-doped CsI + SiPM crystal calorimeter. *Nucl. Instrum. Meth. A* **2019**, *936*, 94–97. [CrossRef]

3. Atanov, N.; Baranov, V.; Borrel, L.; Bloise, C.; Budagov, J.; Ceravolo, S.; Cervelli, F.; Colao, F.; Cordelli, M.; Corradi, G.; et al. The Mu2e crystal calorimeteer: An overview. *Instruments* **2022**, *6*, 60. [CrossRef]
4. Available online: https://www.hamamatsu.com/jp/en.html (accessed on 18 October 2022).
5. Gioiosa, A.; Bonventre, R.; Donati, S.; Flumerfelt, E.; Horton-Smith, G.; Morescalchi, L.; Rivera, R.A. *Online DAQ and Slow Control Interface for the Mu2e Experiment*; Fermi National Accelerator Lab. (FNAL): Batavia, IL, USA, 2022.
6. Pedreschi, E.; Cervelli, F.; Di Falco, S.; Donati, S.; Morescalchi, L.; Raffaelli, F.; Sarra, I. The DIgitizer ReAdout Controller (DiRAC) of the Mu2e electromagnetic calorimeter at Fermilab. *PoS* **2020**, *119*. [CrossRef]
7. Morescalchi, L.; Cervelli, F.; DiFalco, S.; Donati, S.; Gioiosa, A.; Pasciuto, D.; Sarra, I. *The Readout Electronics of the Mu2e Electromagnetic Calorimeter at Fermilab*; Fermi National Accelerator Lab. (FNAL): Batavia, IL, USA, 2022.
8. Cordelli, M.; Cervelli, F.; Diociaiuti, E.; Donati, S.; Donghia, R.; Di Falco, S.; Spinella, F. Pre-production and quality assurance of the Mu2e calorimeter Silicon Photomultipliers. *Nucl. Instrum. Meth. A* **2018**, *912*, 347–349. [CrossRef]
9. Available online: https://www.anl.gov (accessed on 16 October 2022).
10. Bloise, C.; Ceravolo, S.; Cervelli, F.; Colao, F.; Cordelli, M.; Corradi, G.; Di Falco, S.; Diociaiuti, E.; Donati, S.; Ferrari, C.; et al. An automated QC station for the calibration of the Mu2e calorimter Readout Units. *Nucl. Instrum. Method A* 2022, *submitted*.
11. Available online: http://www.fusione.enea.it/LABORATORIES/Tec/FNG.html.it (accessed on 16 October 2022).